iJRASET
International Journal For Research in Applied Science and Engineering Technology

INTERNATIONAL JOURNAL FOR RESEARCH

IN APPLIED SCIENCE & ENGINEERING TECHNOLOGY

Volume: 11 **Issue:** VII **Month of publication:** July 2023

DOI: https://doi.org/10.22214/ijraset.2023.54783

www.ijraset.com

Call: 08813907089 | E-mail ID: ijraset@gmail.com

International Journal for Research in Applied Science & Engineering Technology (IJRASET)
ISSN: 2321-9653; IC Value: 45.98; SJ Impact Factor: 7.538
Volume 11 Issue VII Jul 2023- Available at www.ijraset.com

Improving Gas Turbine Efficiency through Ribbed Channel Designs: A CFD-Based Study

Shantanu Shanu Singh Parmar[1], Gouraw Beohar[2](Guide), Dr. Shailesh Gupta[3]
[1, 2, 3]*Department of Mechanical Engineering, Shri Ram Institute of Technology, Jabalpur (M.P.), India*

Abstract: ***In order to increase performance and efficiency, this research article investigates the usage of ribbed channels in gas turbines. It uses computational fluid dynamics (CFD) simulations to assess various rib shapes and attack angles and evaluate the thermal-hydraulic performance of ribs. According to the results, square-shaped ribs consistently perform better than alternative rib geometries in terms of efficiency, normalized skin friction coefficient ratio, and skin friction coefficient ratio. The work emphasizes how crucial metal temperature prediction is in gas turbine blades and vanes because of the complex interaction between fluid dynamics and flow. The results may be used to establish and optimize cooling plans for increased gas turbine performance and efficiency.***

Keywords: Gas turbine, rib geometries, attack angle, cooling strategies etc.

I. INTRODUCTION

Gas turbines are essential in today's industrialised world for supplying the rising energy and electricity needs. Over the past fifty years, efficient cooling strategies have been used to increase thermal efficiency and power production. Gas turbine parts with smooth passageways to complicated geometries with unique surfaces and fluid-surface interactions have all been cooled using single-phase gas internal convection. Maximising the total cooling effect while reducing the influence of the thermodynamic power cycle is the main goal.

A high-pressure turbine receives 20% to 30% of compressed air at 650°C from the compressor, which can lower the blades' temperature to around 1000°C for safe engine operation. Innovative key technologies are required for high-temperature turbine blade cooling methods. Predicting metal temperatures for blades and vanes is essential during the design phase to reduce product development cycle time and predict blade and blade life. The intricate flow around the blades and vanes makes it difficult to predict metal temperatures.

Collecting data on hot gas path heat transfer distribution and film cooling data is essential for air foils. Factors such as combustor's high turbulence, acceleration, laminar-to-turbulent transition, film cooling flow, platform secondary flow, and surface roughness all impact vane surface heat transfer. Additionally, factors like leakage, blade tip clearance, and forces like centrifugal and rotational forces must be considered.

Identifying hot spots in the surface of blades and vanes of gas turbines can improve turbine and blade cooling performance. Innovative and new heat transfer data can help identify hot spots and enhance the overall efficiency of gas turbines.

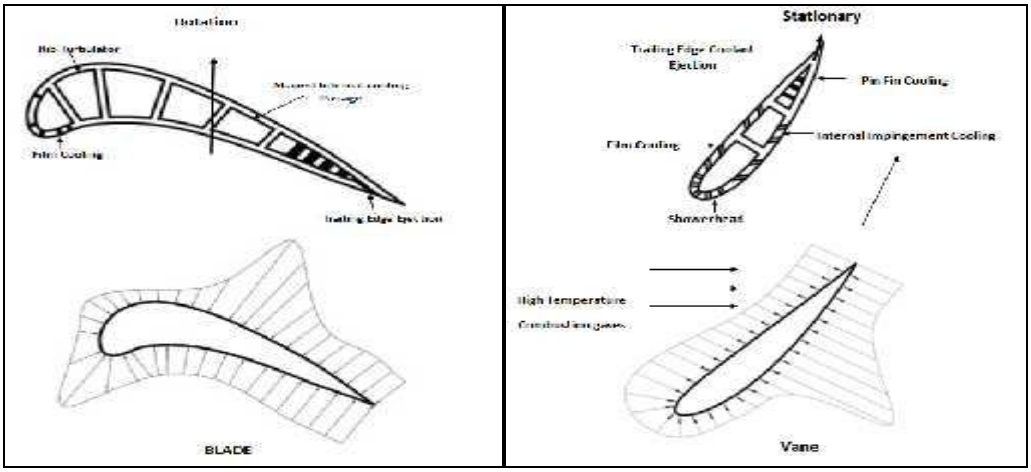

Fig. 1 Cross sectional view and heat flux distribution of (a) vane and (b) blade

Numerous methods have been developed to improve heat transfer in turbine blades and vanes. Jet impingement, film cooling, pin ribs, dimples, and trailing edge potion are used to cool passages in the air foil's center. Combining conventional cooling methods ensures adequate cooling of blades and vanes. Understanding flow physics is crucial for effective cooling. In 2021, Liu, Hussain, Wang and colleagues conducted an experimental study using liquid crystal thermography (LCT) to measure the surface temperature of a rectangular cooling channel with 90° perforated ribs.

Zhu, Chang, Chen and others (2020) used computational fluid dynamics (CFD) to study the effect of channel geometry on a microchannel heat sink with rectangular grooves and ribs using Fluent software. Sharma, Tariq and colleagues used numerical simulation and experimental methods such as ANSYS ICEM, LCT and commercial FLUENT software to model the flow field, turbulence and surface temperature distribution in the ribs channel. Experimental studies by Alfarawi, Abdel-Moneim (2017) and Singh, Ekkad (2017) investigated heat transfer and flow friction in rectangular ducts with various ribs geometries using a dedicated test rig and liquid crystal thermography. Numerical simulations using CFD and Fluent software by Zheng, Wang (2019), Xie, Liu, Yan (2017), Navaei, Mohammed, Munisamy, Yarmand, Gharehkhani (2015), Kamali, Binesh (2008) carried out by various researchers such as Analyze fluid flow, heat transfer properties, and pressure drop in ribsned channels and micro heat sinks.Other methods used in the reviewed studies include transient heat transfer experiments, numerical investigations and custom-made software.

A. Introduction About Rib Turbulent Cooling

Ribs are turbulence promoters placed in pressure and suction sides of internal cooling passages to enhance heat transfer in blades and vanes of advanced gas turbines. These ribs adapt to external loads and isolate fluid stream lines, allowing flow separation and reattachment, as shown in Figure 2.

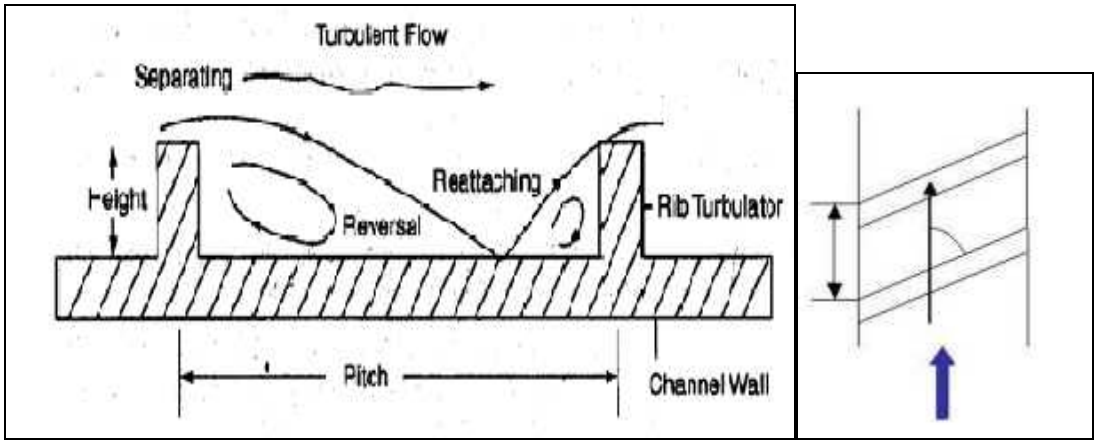

Fig 2. Flow separation and reattachment around ribs

Separation and reattachment increase the flow's turbulence and disturb the boundary layer. This combines cooler elements in the middle of the flow with liquid elements near the walls. Improved heat transfer is caused by two phenomena.

Conduction moves heat from the outer pressure and suction sides of the turbine blades into the inner zone. Internal cooling removes this heat. Most of the time, internal cooling channels are modelled as small sized square or rectangular channels with different aspect ratios. The heat transfer coefficient is influenced by a number of geometric parameters, according to numerous studies. These parameters include the rib's angle of attack, inter-rib placement, rib’s pitch to rib’s height ratio, aspect ratio and block ratio.

In numerous applications, such as compact heat exchangers and gas turbine cooling systems, regular ribs are frequently used in various ducts to enhance the heat transfer process. The thermal and hydraulic performance of these channels is significantly affected by the configurations of these ribs. Due to the improved longitudinal secondary flow, angled ribs outperform vertical ribs in terms of heat transfer and pressure loss. The ribs used in this study have three distinct cross-sections and three distinct rib attack angles—35°, 45°, and 55°. Additionally, the base paper (Liu et al., 2015) and the results of the computational fluid dynamics (CFD) results can be utilized routinely during the design phase to assist in the prediction of sheet performance. This work makes use of a rectangular channel with a 5-aspect ratio (AR). It is assumed that pitch to rib height (P/e) is 10. The experiment's Reynolds numbers fall into the turbulent range and steady state is used for this experiment.

B. Basics of Turbine Cooling

Gas turbine operation is unintentionally impacted by cooling, despite its necessity.

1) The compressor discharges cooling air directly to the vanes and blades. As a result, less mass of air is entering into the combustion chamber.
2) To distinguish between various structures like cooling channels, ribs, and so on, the turbine blade must have a thicker trailing edge, but it has a negative impact on its aerodynamic performance.
3) Different cooling methods are used for different parts of the blade. Typically, the front, also known as the leading edge, is cooled by impingement. Typically, serpentine passages with ribs and localized film cooling are used to cool the central section. Impingement and film cooling are typically used to cool the rear portion, which is referred to as the trailing edge.

C. Types of Cooling

There are two broad categories of cooling used in gas turbine blades.

1) Internal cooling.
2) External cooling.

Types of internal cooling

Over the course of time, numerous variations of internal cooling have been developed. There is no one cooling method that works well for all blades and vanes in all applications. As a result, the cooling scheme should be selected in accordance with the application's requirements and operating conditions.

- *Impingement Cooling:* Impingement cooling is commonly referred to as impingement cooling due to the placement of the cooling air jets close to the leading edge of the airfoil that is impacting the inside surface of the blade. The middle of the blades and vanes can also be cooled with these methods. The surface area of blades and vanes, the size and distribution of the jet holes and the cross section of the cooling channels all of these factors will influence the heat transfer properties of this cooling method.
- *Pin Ribs Cooling:* This method is known as pin ribs cooling because the blade's trailing edge is so narrow that it is hard to machine holes or passages there, that's why pin ribs cooling is often used in this area. The flow around a cylinder and a pin are similar. The wake is dumped downstream as the airflow splits. Additionally, horseshoe-shaped vortices that wrap around the ribs are formed, enhancing heat transfer and facilitating additional mixing. The types of rib array, pin spacing within the array, shape and size of pin all have a significant impact on the properties of heat transfer.
- *Dimple Cooling:* This kind of cooling happens because of the presence of dents or dimples on the surface of the vanes and blades of gas turbine. They improve heat transfer by causing flow separation and reattachment. Because of its low pressure drop, it is a highly desirable refrigeration technology.
- *Turbulent Cooling of Ribs:* The use of turbulence-enhancing structures in the walls of the air-foil's cooling passages, which are cast with the air-foil during manufacturing, is necessary for this type of cooling of ribs. Heat travels through the blade wall to the coolant that flows inside the blade. The coolant flow's Reynolds number, the configuration of the ribs, and the aspect ratio of the channel all have a significant impact on the characteristics of heat transfer. This study investigates the coefficient of friction, Nusselt number, ribbed channel Nusselt number, ribbed channel friction coefficient, and thermal-hydraulic coefficients for different rib sections and attack angles in 2000 Reynolds numbers. It also examines the ratio of ribbed channel friction coefficient to smooth channel friction coefficient, and thermal-hydraulic coefficients for different rib sections and attack angles. The results provide valuable insights into the behavior of ribs in various situations.

D. Equations Relating to Fluid Motion

The continuity and momentum equations, which are used to describe the conservation of mass and momentum, are the two primary types of equations used to describe the flow of fluids. Momentum equations are more commonly referred to as the Navier-Stokes equations. A different set of equations are used to represent energy conservation for flows with heat transfer. The continuity equation is created by applying the law of conservation of mass to a small fluid differential volume. Three equations of the following form are found in Cartesian coordinates: [Ansys fluent user guide page No. 264]

$$\frac{\partial \rho}{\partial t} + \nabla . (\rho \vec{v}) = S_m \quad \text{Equation 1}$$

ISSN: 2321-9653; IC Value: 45.98; SJ Impact Factor: 7.538
Volume 11 Issue VII Jul 2023- Available at www.ijraset.com

The CFD post processor's metrics are listed in the table below, along with this metric and its allowed values. Due to the discretization of the transition and body force terms, values outside the proposed tolerance range add to the error sources.
The equation mentioned above is a general form of equation of mass conservation and is applicable to both compressible and incompressible types of flow. The mass that is added to the dispersed second phase is Source 'Sm'. The momentum equation for a liquid's differential volume can be found by applying Newton's second law of motion. Now, as stated by Newton in his second law of motion, the rate of change of momentum for various liquid volumes is directly proportional to the sum of all external forces acting on that volume. The momentum equation that results in Cartesian coordinates has the following general form: -

$$\frac{\partial}{\partial t}(\rho\vec{v}) + \nabla.(\rho\vec{u}\vec{v}) = -\nabla P + \nabla\bar{\bar{\tau}} + \rho\vec{g} + \vec{F} \qquad \textit{Equation 2}$$

Where P is the static pressure, τ is the stress tensor (explained below), g and F are the gravitational body force and external body force, respectively.

$$\bar{\bar{\tau}} = \mu\left[(\nabla\vec{v} + \nabla\vec{v}^{T}) - \frac{2}{3}\nabla.\vec{v}I\right] \qquad \textit{Equation 3}$$

where I is the unit tensor and μ is the molecular viscosity. The second term on the right is the effect of volumetric expansion.
The first law of thermodynamics states that the rate of change of energy in a fluid particle is equal to the rate of heat input in the fluid particle and work done by the fluid particle. This is how the energy equation is derived. The general form of the resulting energy equation is given as:-

$$\frac{\partial}{\partial t}(\rho E) + \nabla.\left(\vec{v}(\rho E + P)\right) = \nabla.\left(k_{eff}\nabla T - \sum_j h_j\vec{J_j} + (\bar{\bar{\tau}}_{eff}.\vec{v})\right) + S_h \qquad \textit{Equation 4}$$

where keff is the effective conductivity (k + ki), where ki is the turbulent thermal conductivity described according to the turbulence model used) and the diffusive flux of species j. The first three terms on the right-hand side of equation 5 represent the energy transfer due to conduction, species diffusion, and viscous dissipation. This equation includes heat from chemical reactions and all other volumetric heat sources
In equation 5, the energy per unit mass E is described as

$$E = h - \frac{P}{\rho} + \frac{u^2}{2} \qquad \textit{Equation 5}$$

II. METHODOLOGY AND APPROACH

The methodology formulated for carrying out the objectives which I discussed in the previous chapter consist of following shown in steps:

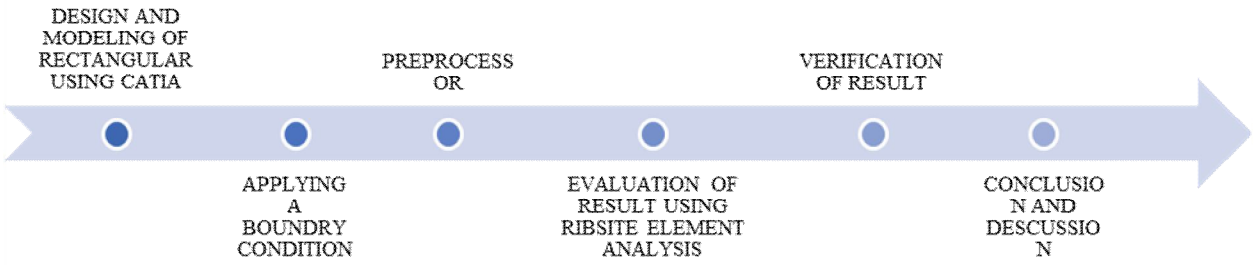

Figure 1 Flow chart of the design process

A. Methodology and CFD Governing Equation

A rectangular duct with a rectangular cross-section of 200 x 40 mm2 and a duct length of 550 mm was considered in this study. The bottom of the square duct is provided with an aluminium plate with 10 ribs along the surface of the square duct. 3 different rib attack angles 35°, 45° and 55° and 3 different rib cross section shapes are used. The cross-sectional area of each model is the same and is equal to 4 mm² for each individual model and that the underside of the panel is kept under a uniform heat flux of 1000 W/m2. The air was passed through the duct at various Reynolds numbers from 8000 to 18000 in 2000 steps with their corresponding velocities ranging from 1.77 m/s to 3.98 m/s in 6 steps.

B. Physical Models

In this study, a rectangular duct with a length (L) of 550 mm, a width (W) of 200 mm, and a height (H) of 38 mm is included in the analysis. The hydraulic diameter (Dh) of each channel is 66 mm. A plate with numerous ribs is provided at the bottom of the rectangular duct. Various models of rectangular ducts have been produced, each with different rib cross-sections and rib attack angles. Rib attack angle for individual models should be 35°.45° and 55° with a zigzag gap in the rib path. (Liu et al., 2018; Singh & Ekkad, 2017; N. Zheng et al., 2015)

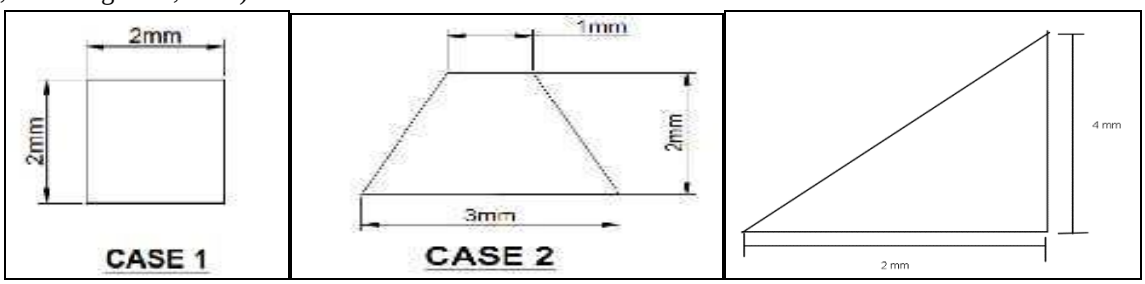

Case1 Square shaped | Case 2 Isosceles trapezoidal shape | Case 3 Right angle triangle shape

The figure shown below is a 3d model of a rectangular channel with a width of 200 mm, channel height of 38 mm, channel length of 550 mm.

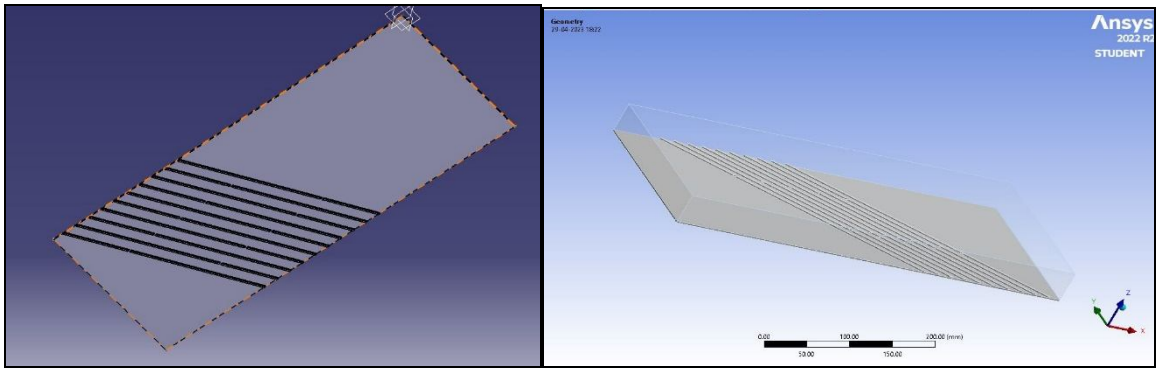

Fig4. 3D Mode of Al plate created in a CATIA V5 R21

Fig5. Creation of a Fluid domain in an Al sheet

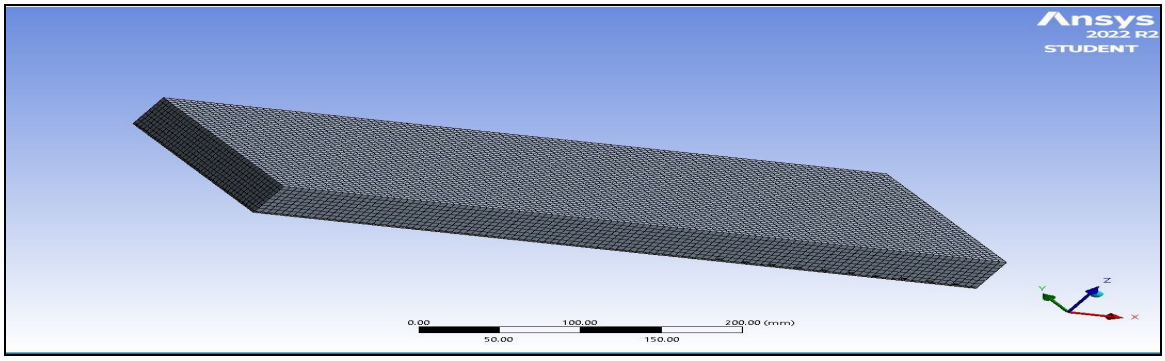

Fig.6 Mesh generation information

This metric and its allowed values are shown in the table below, along with the metrics available via the CFD post processor. Values outside the proposed tolerance range add to the sources of error due to the discretization of the transition and body force terms.

Nodes	Elements
58569	293682

The numerical analysis of air flowing through a rectangular duct with internal ribs of varying rib's attack angles and varying rib's cross-sectional shape cases of the same cross section area and an aluminum plate covering the bottom portion. Using the following parameters, a comparison of analysis has been carried out for a variety of cases: Thermal Hydraulic Performance Factor, Skin friction coefficient factor, Skin friction coefficient factor Ratio (i.e., skin friction coefficient of ribbed channel/skin friction coefficient of smooth channel), and Nusselt number (i.e., Nusselt number for ribbed channel/Nusselt number for smooth channel). The plate's opposite end is then subjected to a constant heat flux of 1000 W/m2.

C. The Parameters which Are Analysed in This Study

1) *Reynolds Number (Re):* The Reynolds number is a dimensionless number described as the ratio of the inertial force (ρ u L) to the viscous or frictional force (μ) and expressed as:

$$\mathbf{Re = \rho V D_h / \mu} \qquad \text{Equation 6}$$

where ρ is the density (kg/m3), μ is the dynamic viscosity (Ns/m2), ν is the dynamic viscosity, V is the average velocity of the fluid, and Dh is the hydraulic diameter of the geometry. The higher the Reynolds number, the more turbulent the flow.

2) *Nusselt Number (Nu):* The Nusselt number is a measure of convective heat transfer occurring at a surface and is described as:

$$\mathbf{Nu = hD_h/k} \qquad \textit{Equation 7}$$

where h is the convective heat transfer coefficient (W/m2xK), Dh is the pipe diameter, and k is the thermal conductivity of the fluid.

- Note: Nusselt number for rectangular smooth-surfaced ducts, rib less (Nu_o), calculated by the standard Dittus-Boelter equation (theoretically).

$$\mathbf{Nu_o = 0.023\, Re^{0.8}\, Pr^{0.4}} \qquad \textit{Equation 8}$$

- We have taken the case of a smooth-surfaced duct as a reference.

3) *Skin Friction Coefficient Factor (f):* Friction coefficient is the frictional energy loss in a duct based on fluid velocity and frictional resistance.

$$f = \frac{2 \quad \Delta P}{(L/D)\ \rho U^2} \qquad \textit{Equation 9}$$

Where Dh is Hydraulic Diameter and U is mean air velocity at inlet

- Note: Friction coefficient of a rectangular smooth surface duct, i.e. Ribless (Fro) is calculated by the Blasius formula.

$$\mathbf{fro = 0.079\, Re^{-0.25}} \qquad \text{Equation 1}$$

4) *Thermal Hydraulic Performance Factor (η):* It is described by the following equation and is analogous to improved heat transfer at constant pump power.

$$\mathbf{\eta = (Nu_r / Nu_o) / \{ (f_r / f_o) \text{ ^ } (1/3) \}} \qquad \textit{Equation 11}$$

where Nu_r, fr, Nu_0, and f_0 are the Nusselt numbers and friction coefficients for ribbed and ribbed duct configurations, respectively.

III. RESULT AND DISCUSSION

A. Nusselt Number Ratio:

the table representing the given data about a right-angle triangle at different velocity, and the columns represent the corresponding values of (Nur/Nuo) at angles 35, 45, and 55 degrees.

1) *Case 1 (Square Shaped)*

Square shaped			
Velocity (m s^-1)	(Nur/Nuo) at 35	(Nur/Nuo) at 45	(Nur/Nuo) at 55
1.77	1.192109242	1.12514903	1.114295068
2.21	1.18120184	1.128957852	1.115245894
2.65	1.163168109	1.125410788	1.109836102
3.1	1.140346159	1.115513122	1.099534663
3.54	1.119846725	1.102663392	1.08692509
3.98	1.102927512	1.08919513	1.074139707

Table 1 representing the smooth, square ribs with different inlet velocities and Surface Nusselt number

2) Case 2 (Isosceles Trapezoidal Shaped)

Isosceles Trapezoidal Shaped			
Velocity (m s^-1)	(Nur/Nuo) at 35	(Nur/Nuo) at 45	(Nur/Nuo) at 55
1.77	1.176584783	1.128239173	1.072355495
2.21	1.171573369	1.129476613	1.075021163
2.65	1.161506538	1.122880459	1.070541397
3.1	1.148207885	1.11212541	1.062040467
3.54	1.133410108	1.100670005	1.052192302
3.98	1.11865645	1.088859215	1.042024006

Table 2 representing the smooth, Isosceles Trapezoidal Shaped with different inlet velocities and Surface Nusselt number

3) Case 3 (Right angle triangle Shaped)

Right angle triangle			
Velocity (m s^-1)	(Nur/Nuo) at 35	(Nur/Nuo) at 45	(Nur/Nuo) at 55
1.77	1.114485579	1.113124514	1.137971357
2.21	1.115012706	1.11392431	1.139260134
2.65	1.108846466	1.107822723	1.13336115
3.1	1.098778283	1.09784214	1.123249595
3.54	1.087382762	1.08635849	1.111482619
3.98	1.075911715	1.074974867	1.099854544

Table 3 representing the smooth, and Right-angle Triangle Shaped with different inlet velocities and Surface Nusselt number

B. Ratio of Skin friction coefficient with ribbed channel to Skin friction coefficient with smooth channel Change in (f_r/f_o) with respect to Velocity

The table representing the square Shaped and Isosceles Trapezoidal Shaped ribs with different inlet velocities and Friction ratio for different rib attack angle in Al plate:

the table shown below the square Shaped ribs with different inlet velocities and Friction ratio for different rib attack angle in Al plate:

1) Friction ratio for different rib attack angle for case 1 (Square Shaped)

Square shaped			
Velocity (m s^-1)	fr/fo for 35	fr/fo for 45	fr/fo for 55
1.77	1.026515485	0.999510876	1.054435181
2.21	1.008334226	0.990202374	1.039727725
2.65	0.98937255	0.980473753	1.022884135
3.1	0.972561995	0.972342348	1.007147631
3.54	0.9591679	0.966200035	0.994336279
3.98	0.948334651	0.961261784	0.983188948

Table 4 Represents Friction ratio for different rib attack angle for case 1 (Square Shaped)

Ratio of Skin friction coefficient with ribbed channel to Skin friction coefficient with smooth channel (f_r/f_o) Vs Velocity (case 1)

2) Friction ratio for different rib attack angle for case 2 (Isosceles Trapezoidal Shaped)

The table shown below the Isosceles Trapezoidal Shaped ribs with different inlet velocities and Friction ratio for different rib attack angle in Al plate:

Isosceles Trapezoidal Shaped			
Velocity (m s^-1)	fr/fo for 35	fr/fo for 45	fr/fo for 55
1.77	1.121033346	1.036606715	1.003923526
2.21	1.104297254	1.020896903	0.986182427
2.65	1.084537961	1.003262115	0.967533205
3.1	1.067389264	0.986653474	0.951224455
3.54	1.05328295	0.97420542	0.938415339
3.98	1.041622674	0.964031399	0.928370923

Table 5 Represents Friction ratio for different rib attack angle for case 2 (Isosceles Trapezoidal Shaped ribs)

Ratio of Skin friction coefficient with ribbed channel to Skin friction coefficient with smooth channel (f_r/f_o) Vs Velocity (case 2)

3) Friction ratio for different rib attack angle for case 3 (Right angle triangle shaped)

Right angle triangle			
Velocity (m s^-1)	fr/fo for (35°)	fr/fo for (45°)	fr/fo for (55°)
1.77	1.06554139	1.064352649	1.005512764
2.21	1.048303072	1.047513804	0.987227704
2.65	1.030071461	1.029557642	0.96943928
3.1	1.013965066	1.01356361	0.954463215
3.54	1.001471335	1.000930651	0.942576635
3.98	0.991487133	0.990973846	0.93351803

Table 6 Ratio of Skin friction coefficient with ribbed channel to Skin friction coefficient with smooth channel (f_r/f_o) Vs Velocity (case 3)

IV. COMPARISONS OF RESULTS

1) *Case 1 (Square Shaped Ribs):* The ribs findings for Case 1 are shown in the graph's conclusion, with a concentration on square-shaped shapes. The results offer important new understandings of the relationships among velocity, angle of attack, skin friction coefficient ratios and (Nu_r/Nu_o), skin friction coefficient ratios normalized by the cube root of the freestream velocity (f_r/f_o)^(1/3)).

Graph 1 shown below comparison of Skin friction Ratio to velocity for Square Shaped ribs for different attack angle

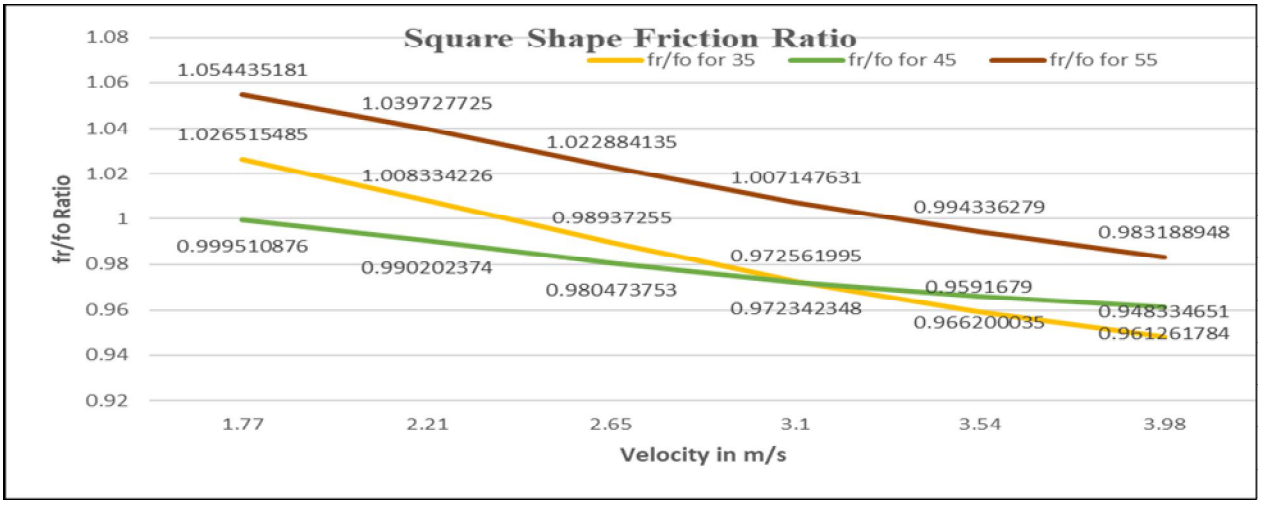

ISSN: 2321-9653; IC Value: 45.98; SJ Impact Factor: 7.538
Volume 11 Issue VII Jul 2023- Available at www.ijraset.com

Graph 2 shown below comparison of (Nu_r/Nu_o) Ratio to velocity for Square Shaped Shape ribs for different attack angle

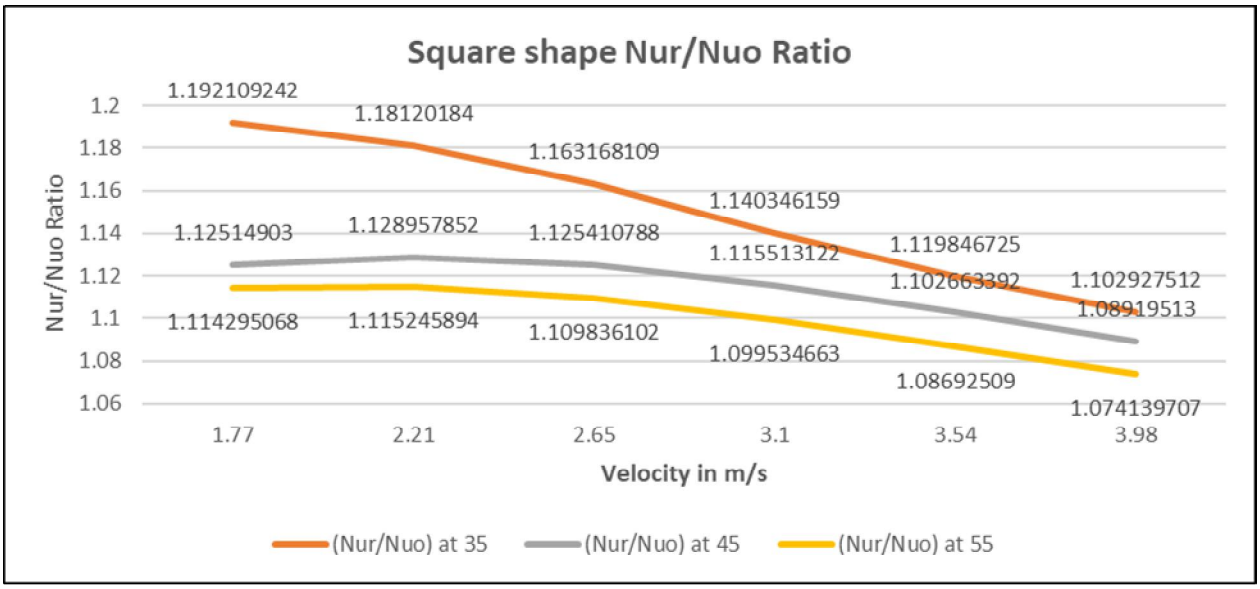

According to the statistics, the skin friction coefficient ratio at all three angles of attack (35°, 45°, and 55°) somewhat decreases as the velocity rises. The (f_r/f_o)^(1/3) numbers also indicate a modest decrease as the velocity increases. These ribs findings imply that the skin friction produced is slightly less effective as the square-shaped shape moves at a quicker speed.

2) *Case 2 (Isosceles Trapezoidal Shaped):* The graph concludes by summarizing the research results for Case 2, concentrating on isosceles trapezoidal-shaped shapes. By analyzing the velocity, skin friction coefficient ratios (Nu_r/Nu_o), normalized skin friction coefficient ratios ((f_r/f_o)^(1/3)), and efficiency (η) at various angles of attack (35°, 45°, and 55°), the results offer significant new insights into the aerodynamic properties of these shapes.

Graph 3 shown comparison of Skin Friction Ratio using Isosceles Trapezoidal Shaped Shape ribs for different attack angle:

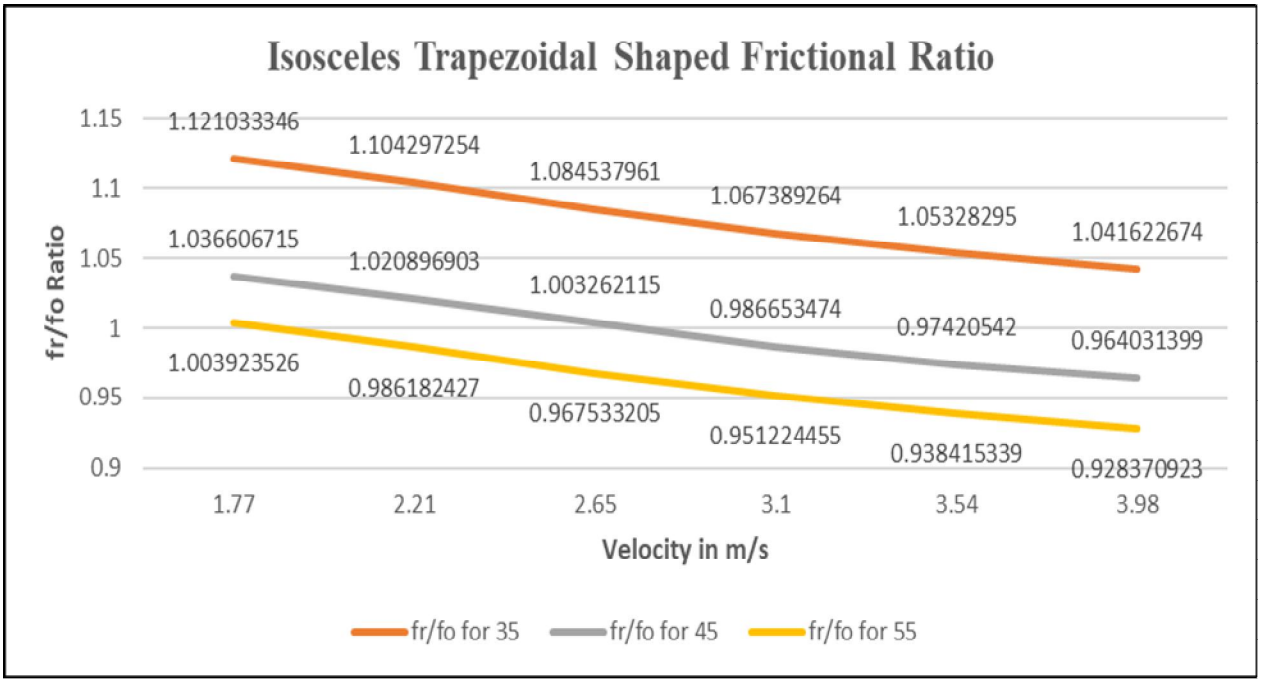

Graph 4 shown below comparison of (Nu_r/Nu_o) Ratio to velocity for on isosceles trapezoidal-shaped ribs for different attack angle

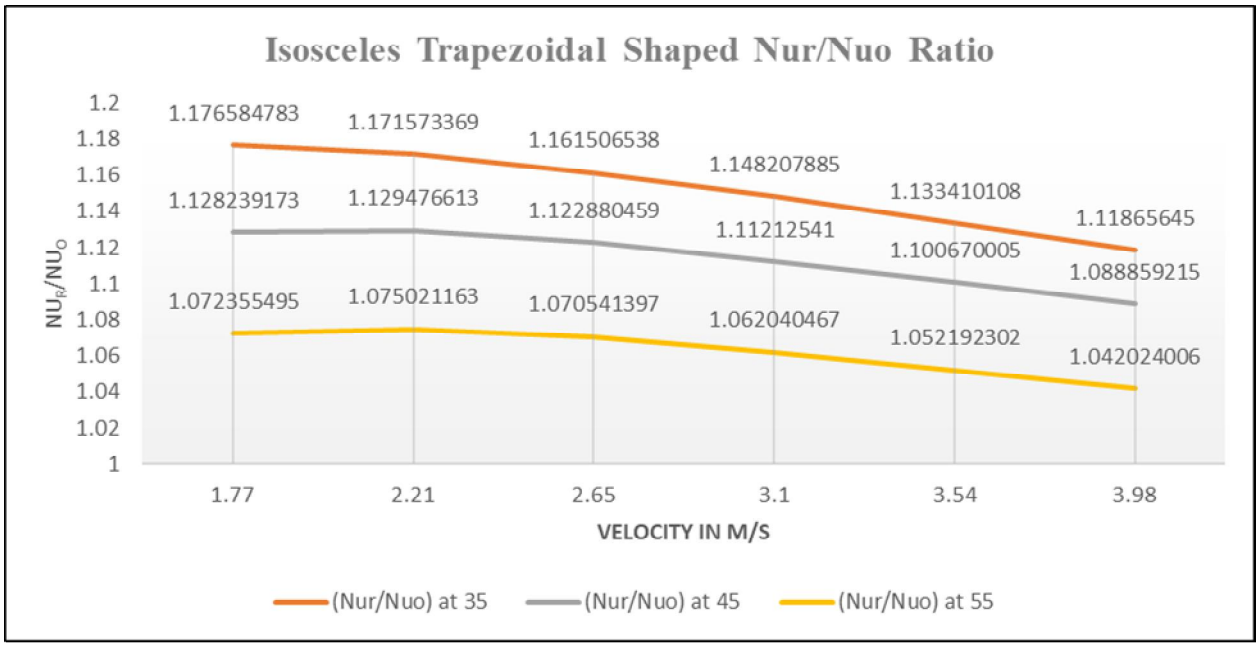

The research shows that the skin friction coefficient ratios at all three angles of attack somewhat decrease as the velocity rises. This shows that as the velocity rises, the efficiency of the skin friction produced by isosceles trapezoidal shapes significantly decreases. A falling trend in the skin friction efficiency relative to the cube root of the freestream velocity is also shown by the normalized skin friction coefficient ratios ((f_r/f_o)^(1/3)), which gradually decrease as the velocity increases.

3) *Case 3(Right-Angle Triangle):* The accompanying table, which concentrates on shapes with a right-angle triangle form, concludes with summarizing the results for Case 3. By analyzing the velocity, skin friction coefficient ratios (Nu_r/Nu_o), normalized skin friction coefficient ratios ((f_r/f_o)^(1/3)), and efficiency (η) at various angles of attack (35°, 45°, and 55°), the ribs findings provide insight into these shapes' aerodynamic properties.

Graph 5 Graphs shown comparison of Skin Friction Ratio using Right angle triangle shape ribs for different attack angle:

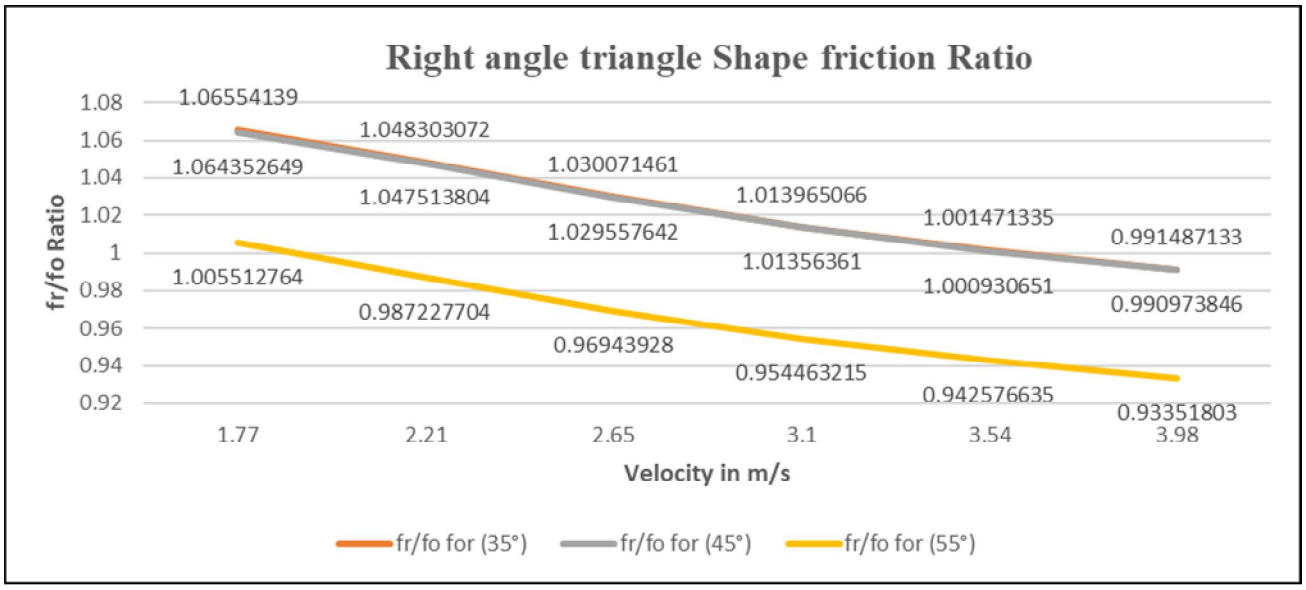

Graph 6 shown below comparison of (Nu_r/Nu_o) Ratio to velocity for on Right-angle triangle shape ribs for different attack angle

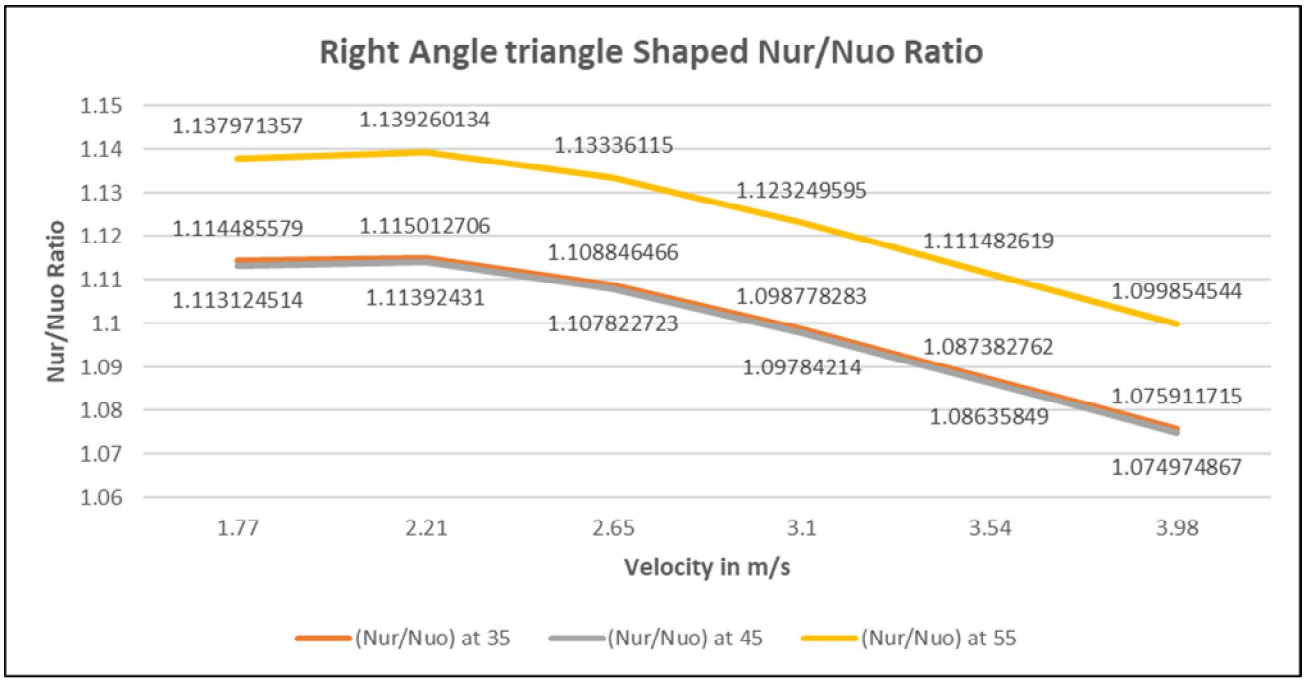

The research shows that the skin friction coefficient ratios at all three angles of attack change very little as the velocity rises. This implies that the skin friction produced by shapes with right-angle triangle ribs remains mostly constant as the velocity varies. Additionally, when the velocity increases, the normalized skin friction coefficient ratios ((f_r/f_o)^(1/3)) show a tiny decrease, showing a minor decline in skin friction efficiency compared to the cube root of the freestream velocity.

C. Performance Factor (η)

The Nusselt ratio and friction ratio have an impact on the thermal hydraulic Performance factor, as was covered in the preceding chapter. Below is a connection between the thermal performance factor:

$$\eta = \left(\frac{\frac{Nur}{Nuo}}{\left(\frac{fr}{fo}\right)^{1/3}} \right)$$

In the 10,000–16,000 Reynolds number range, case 2 has a higher thermal hydraulic performance factor than case 1, according to a comparison between the two cases. Thermal hydraulic Performance factor for case 1 is larger than that of case 2 at a Reynolds number of 8,000, nevertheless. The graph also shows that when the Reynolds number rises, the thermal hydraulic performance factor falls.

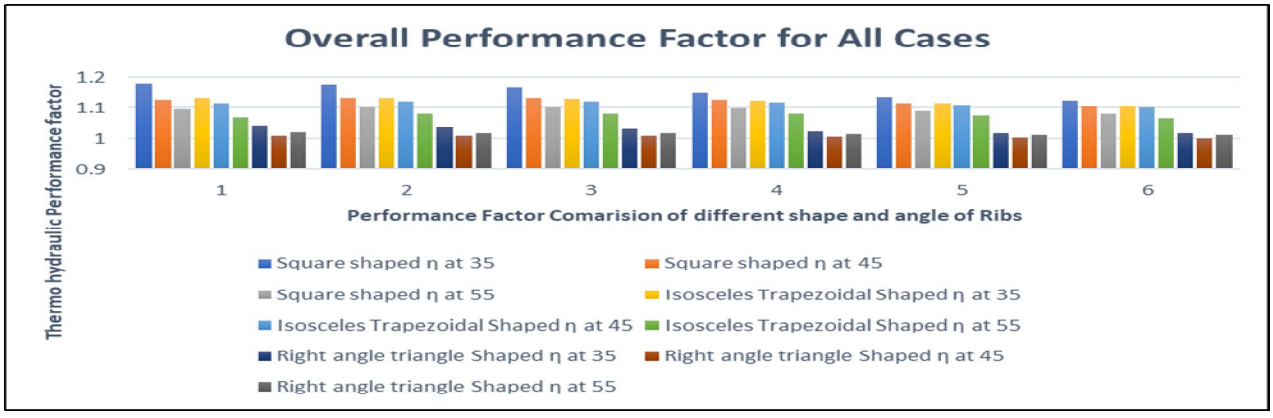

Graph 7 Comparison of Thermal hydraulic Performance factor (η)(at different rib attack angle for case1 case2 and case 3)

V. CONCLUSION

A comprehensive analysis of results for different cases reveals the most important results and observations for each case.

1) For case 1, a square object, analysis shows that the ratio of normalized downward velocity (Nu_r/ Nu_o) at different angles (35°, 45°, 55°) decreases as velocity increases. is shown. Similarly, the value of (fr/fo)^(1/3) also decreases with increasing speed. The value of η, which represents efficiency, also decreases as speed increases.

2) A similar trend is observed in case 2, observing an isosceles trapezoidal object. The (Nu_r/ Nu_o) ratio decreases with increasing velocity, and so do the values of (fr/fo)^(1/3) and η. However, the (Nu_r/Nu_o) values remained constant at various angles, suggesting that the shape of the object does not significantly affect the downstream velocity.

3) In Case 3, a right-triangular object, the (Nu_r/ Nu_o) ratio decreases with increasing velocity, as in the previous case. The values of (fr/fo)^(1/3) and η also decrease with increasing velocity. Again, object geometry does not seem to have a significant effect on downstream velocity. Overall, the analysis found that increasing velocity decreased downstream velocity and also decreased object efficiency. Object shape has little effect on these trends. These results provide valuable insight into the hydrodynamics of different bodies at different velocities.

a) Results Findings More focus on Some comparisons can be made when analysing the results for all three cases: square, isosceles trapezoid, and right triangle objects.

b) Regarding the skin friction coefficient ratio (Nur/Nuo), the square object always shows higher values than the other two cases, even at different velocities and angles of attack.

c) This suggests that square objects are more capable of generating skin friction under the conditions tested.

d) Considering the normalized skin friction coefficient ratio (fr/fo^(1/3)), square bodies always have higher values than isosceles, trapezoids and right triangles.

e) This indicates that the square body has a higher skin friction efficiency than the cube root of the free stream velocity.

f) In terms of overall efficiency (η), square bodies consistently achieve higher efficiency values compared to isosceles, trapezoids, and right-triangular bodies.

g) This suggests that square objects are more efficient at converting input energy into usable skin friction.

h) Based on a comparison of the three cases, square objects consistently outperform other shapes in terms of Skin friction coefficient ratio, normalized skin friction coefficient ratio, and efficiency.

Therefore, square objects are considered to be the best results among the shapes tested in this study.

However, it is important to note that these conclusions are based on certain conditions and assumptions of our analysis. This leads to the conclusion that a channel's thermal hydraulic performance factor is higher when the rib attack angle is lower.

REFERENCES

[1] Alfarawi, S., Abdel-Moneim, S. A., & Bodalal, A. (2017). Experimental investigations of heat transfer enhancement from rectangular duct roughened by hybrid ribs. International Journal of Thermal Sciences, 118, 123–138. https://doi.org/10.1016/j.ijthermalsci.2017.04.017

[2] Aljibory, M., Lafta Rashid, F., Qahtan, H., Wahhab AL-Jibory, M., & Qahtan Hussein, H. (n.d.). Review Of Heat Transfer Enhancement In Air-Cooled Turbine Blades Heat transfer enhancement in ducts View project Natural gas industry View project Review Of Heat Transfer Enhancement In Air-Cooled Turbine Blades. www.ijstr.org

[3] Chung, H., Park, J. S., Park, S., Choi, S. M., Rhee, D. H., & Cho, H. H. (2015). Augmented heat transfer with intersecting rib in rectangular channels having different aspect ratios. International Journal of Heat and Mass Transfer, 88, 357–367. https://doi.org/10.1016/j.ijheatmasstransfer.2015.04.033

[4] Ghani, I. A., Sidik, N. A. C., Mamat, R., Najafi, G., Ken, T. L., Asako, Y., & Japar, W. M. A. A. (2017). Heat transfer enhancement in microchannel heat sink using hybrid technique of ribs and secondary channels. International Journal of Heat and Mass Transfer, 114, 640–655. https://doi.org/10.1016/j.ijheatmasstransfer.2017.06.103

[5] Kamali, R., & Binesh, A. R. (2008). The importance of rib shape effects on the local heat transfer and flow friction characteristics of square ducts with ribbed internal surfaces. International Communications in Heat and Mass Transfer, 35(8), 1032–1040. https://doi.org/10.1016/j.icheatmasstransfer.2008.04.012

[6] Lee, E., Wright, L. M., & Han, J.-C. (2003). GT2003-38900 HEAT TRANSFER IN ROTATING RECTANGULAR CHANNELS (AR = 4:1) WITH V-SHAPED AND ANGLED RIB TURBULATORS WITH AND WITHOUT GAPS. Power for Land. http://www.asme.or

[7] Lee, E., Wright, L. M., & Han, J. C. (2005). Heat transfer in rotating rectangular channels with V-shaped and angled ribs. Journal of Thermophysics and Heat Transfer, 19(1), 48–56. https://doi.org/10.2514/1.9065

[8] Liu, J., Hussain, S., Wang, J., Wang, L., Xie, G., & Sundén, B. (2018). Heat transfer enhancement and turbulent flow in a high aspect ratio channel (4:1) with ribs of various truncation types and arrangements. International Journal of Thermal Sciences, 123, 99–116. https://doi.org/10.1016/j.ijthermalsci.2017.09.013

[9] Liu, J., Hussain, S., Wang, W., Wang, L., Xie, G., & Sundén, B. (2019). Heat transfer enhancement and turbulent flow in a rectangular channel using perforated ribs with inclined holes. Journal of Heat Transfer, 141(4). https://doi.org/10.1115/1.4042841

[10] Liu, J., Hussain, S., Wang, W., Xie, G., & Sundén, B. (2021). Experimental and numerical investigations of heat transfer and fluid flow in a rectangular channel with perforated ribs. International Communications in Heat and Mass Transfer, 121. https://doi.org/10.1016/j.icheatmasstransfer.2020.105083

[11] Liu, J., Xie, G., & Simon, T. W. (2015). Turbulent flow and heat transfer enhancement in rectangular channels with novel cylindrical grooves. International Journal of Heat and Mass Transfer, 81, 563–577. https://doi.org/10.1016/j.ijheatmasstransfer.2014.10.021
[12] Lu, B., & Jiang, P. X. (2006). Experimental and numerical investigation of convection heat transfer in a rectangular channel with angled ribs. Experimental Thermal and Fluid Science, 30(6), 513–521. https://doi.org/10.1016/j.expthermflusci.2005.09.007
[13] Maurer, M., von Wolfersdorf, J., & Gritsch, M. (2007). An experimental and numerical study of heat transfer and pressure loss in a rectangular channel with v-shaped ribs. Journal of Turbomachinery, 129(4), 800–808. https://doi.org/10.1115/1.2720507
[14] Moon, M. A., Park, M. J., & Kim, K. Y. (2014). Evaluation of heat transfer performances of various rib shapes. International Journal of Heat and Mass Transfer, 71, 275–284. https://doi.org/10.1016/j.ijheatmasstransfer.2013.12.026
[15] Navaei, A. S., Mohammed, H. A., Munisamy, K. M., Yarmand, H., & Gharehkhani, S. (2015). Heat transfer enhancement of turbulent nanofluid flow over various types of internally corrugated channels. Powder Technology, 286, 332–341. https://doi.org/10.1016/j.powtec.2015.06.009
[16] Peng, W., Jiang, P. X., Wang, Y. P., & Wei, B. Y. (2011). Experimental and numerical investigation of convection heat transfer in channels with different types of ribs. Applied Thermal Engineering, 31(14–15), 2702–2708. https://doi.org/10.1016/j.applthermaleng.2011.04.040
[17] Qahtan Hussein, H., Wahhab Al-Jibory, M., & Lafta Rashid, F. (n.d.). Heat Transfer Enhancement of Gas Turbine Blades Using Coated Ribs with Nanocomposite Materials. In Journal of Mechanical Engineering Research and Developments (Vol. 43, Issue 6).
[18] Sharma, N., Tariq, A., & Mishra, M. (2019). Experimental Investigation of Heat Transfer Enhancement in Rectangular Duct with Pentagonal Ribs. Heat Transfer Engineering, 40(1–2), 147–165. https://doi.org/10.1080/01457632.2017.1421135
[19] Singh, P., & Ekkad, S. (2017). Experimental study of heat transfer augmentation in a two-pass channel featuring V-shaped ribs and cylindrical dimples. Applied Thermal Engineering, 116, 205–216. https://doi.org/10.1016/j.applthermaleng.2017.01.098
[20] Singh, P., Pandit, J., & Ekkad, S. V. (2017). Characterization of heat transfer enhancement and frictional losses in a two-pass square duct featuring unique combinations of rib turbulators and cylindrical dimples. International Journal of Heat and Mass Transfer, 106, 629–647. https://doi.org/10.1016/j.ijheatmasstransfer.2016.09.037
[21] Tanda, G. (2004). Heat transfer in rectangular channels with transverse and V-shaped broken ribs. International Journal of Heat and Mass Transfer, 47(2), 229–243. https://doi.org/10.1016/S0017-9310(03)00414-9
[22] Wang, J., Liu, J., Wang, L., Sundén, B., & Wang, S. (2018). Numerical investigation of heat transfer and fluid flow in a rotating rectangular channel with variously-shaped discrete ribs. Applied Thermal Engineering, 129, 1369–1381. https://doi.org/10.1016/j.applthermaleng.2017.09.142
[23] Wright, L. M., Fu, W.-L., & Han, J.-C. (n.d.). THERMAL PERFORMANCE OF ANGLED, V-SHAPED, AND W-SHAPED RIB TURBULATORS IN ROTATING RECTANGULAR COOLING CHANNELS (AR = 4:1). http://www.asme.org/about-asme/terms-of-use
[24] Xia, G., Zhai, Y., & Cui, Z. (2013). Numerical investigation of thermal enhancement in a micro heat sink with fan-shaped reentrant cavities and internal ribs. Applied Thermal Engineering, 58(1–2), 52–60. https://doi.org/10.1016/j.applthermaleng.2013.04.005
[25] Xie, G., Liu, X., Yan, H., & Qin, J. (2017). Turbulent flow characteristics and heat transfer enhancement in a square channel with various crescent ribs on one wall. International Journal of Heat and Mass Transfer, 115, 283–295. https://doi.org/10.1016/j.ijheatmasstransfer.2017.07.012
[26] Zhai, Y. L., Xia, G. D., Liu, X. F., & Li, Y. F. (2014). Heat transfer in the microchannels with fan-shaped reentrant cavities and different ribs based on field synergy principle and entropy generation analysis. International Journal of Heat and Mass Transfer, 68, 224–233. https://doi.org/10.1016/j.ijheatmasstransfer.2013.08.086
[27] Zheng, D., Wang, X., & Yuan, Q. (2019a). Numerical investigation on the flow and heat transfer characteristics in a rectangular channel with V-shaped slit ribs. Infrared Physics and Technology, 101, 56–67. https://doi.org/10.1016/j.infrared.2019.06.004
[28] Zheng, D., Wang, X., & Yuan, Q. (2019b). The flow and heat transfer characteristics in a rectangular channel with convergent and divergent slit ribs. International Journal of Heat and Mass Transfer, 141, 464–475. https://doi.org/10.1016/j.ijheatmasstransfer.2019.06.060
[29] Zheng, N., Liu, P., Shan, F., Liu, Z., & Liu, W. (2016). Effects of rib arrangements on the flow pattern and heat transfer in an internally ribbed heat exchanger tube. International Journal of Thermal Sciences, 101, 93–105. https://doi.org/10.1016/j.ijthermalsci.2015.10.035
[30] Zheng, N., Liu, W., Liu, Z., Liu, P., & Shan, F. (2015). A numerical study on heat transfer enhancement and the flow structure in a heat exchanger tube with discrete double inclined ribs. Applied Thermal Engineering, 90, 232–241. https://doi.org/10.1016/j.applthermaleng.2015.07.009
[31] Zhu, Q., Chang, K., Chen, J., Zhang, X., Xia, H., Zhang, H., Wang, H., Li, H., & Jin, Y. (2020). Characteristics of heat transfer and fluid flow in microchannel heat sinks with rectangular grooves and different shaped ribs. Alexandria Engineering Journal, 59(6), 4593–4609. https://doi.org/10.1016/j.aej.2020.08.014

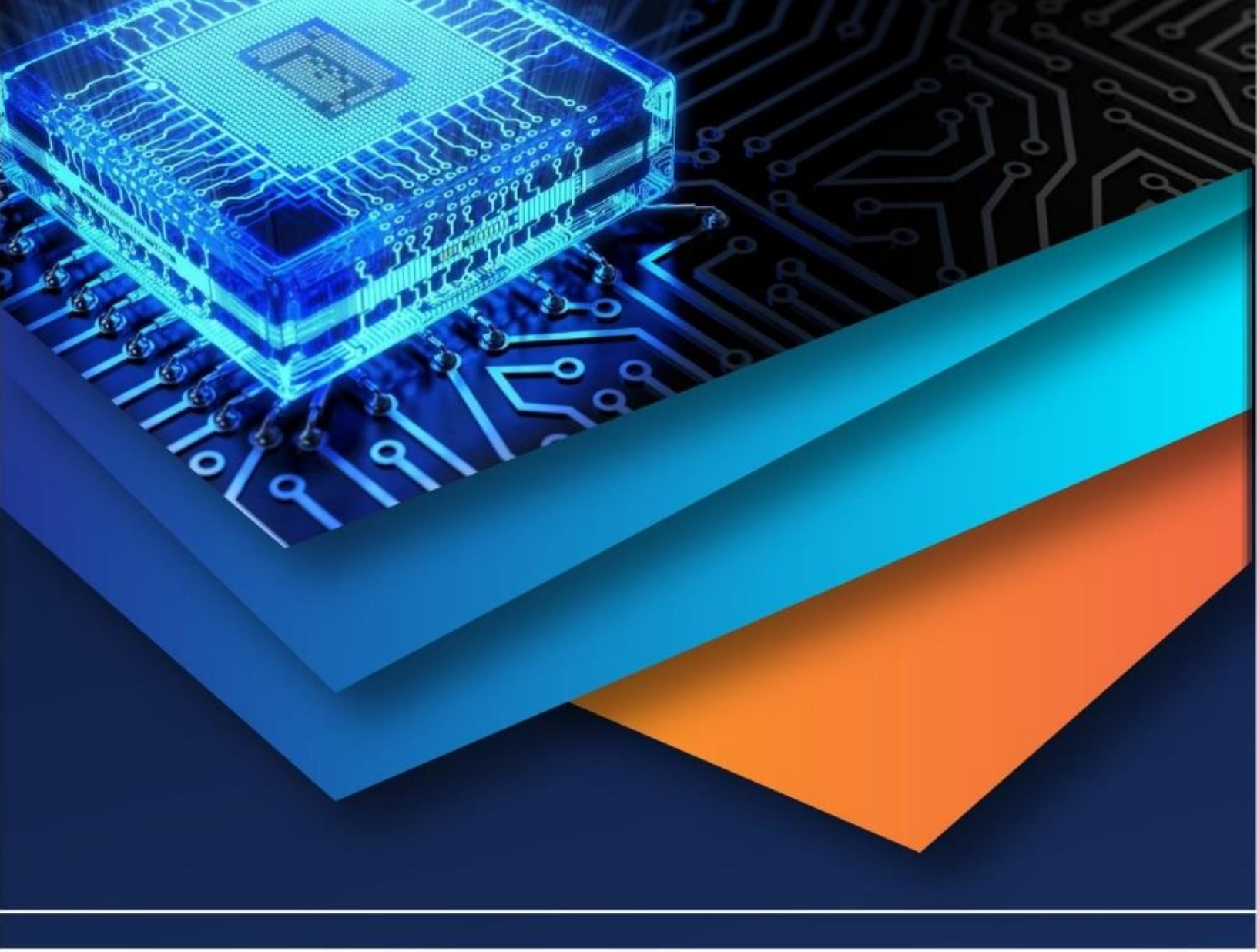

10.22214/IJRASET

45.98

IMPACT FACTOR: 7.129

IMPACT FACTOR: 7.429

INTERNATIONAL JOURNAL FOR RESEARCH

IN APPLIED SCIENCE & ENGINEERING TECHNOLOGY